Influence of noise on dynamics with fractal Fourier spectra

Michael A. Zaks

Department of Nonlinear Dynamics, Institute of Physics
Potsdam University, Postfach 601553, D-14415 Potsdam Germany

Abstract

In deterministic dynamics the processes with fractal power spectra occupy the intermediate position between ordered and chaotic temporal behavior. We study numerically the influence of different kinds of noise upon these processes. In general, under the action of noise the spectral measure becomes absolutely continuous and the correlations decay. However, during the certain intermediate period the autocorrelation retains the pattern which is typical for dynamics with fractal spectra. Duration of this period is related to the noise intensity by the power law.

PACS: 02.30.Nw + 05.45.Df
KEYWORDS: singular continuous spectrum; autocorrelation.

1 Introduction

Fourier analysis of time data is one of the classical tools in the experimental studies of dynamical systems: in the pioneering years of nonlinear dynamics, power spectra served as a robust criterion which allowed to distinguish between the ordered states and the "turbulent" ones [1, 2]. Power spectra of periodic and quasiperiodic states consist of discrete peaks, and the countable set of frequency values which support these peaks, has zero measure. On the contrary, power spectra of typical chaotic and stochastic processes are continuous curves spanned over the intervals of frequency values. In this case, spectral measure is absolutely continuous with respect to the Lebesgue measure.

There exists, however, an intermediate kind of power spectrum, supported neither by a discrete set of points, nor by an interval, but by a fractal set of zero measure. In the context of spectral properties of linear operators, such objects are known under the name of singular continuous spectrum, and are well represented in literature on mathematical physics (see e.g. [3, 4]). In recent years, singular continuous power spectra have been found in certain classes of deterministic dynamical systems where they indicate to the particular kind of dynamics, neither (quasi)periodic, nor chaotic. Among the examples are strange nonchaotic attractors in quasiperiodically driven oscillators [5, 6], systems at the accumulation points of sequences of homoclinic bifurcations [7], flows with irrational rotation numbers on 2-tori with states of equilibrium [8, 9]. In autonomous dynamical systems, two different mechanisms behind singular continuous power spectra were identified [7]. The first one, common for the mappings and flows, is due to the special geometry of the attractor. The second mechanism is of dynamical origin: it is specific for the flows and owes to the presence of saddle points in the attractor. Near the local stable manifold of such points, time intervals between consecutive returns onto the Poincaré surface are unbounded, and the Poincaré mapping does not deliver an adequate picture of the continuous dynamics: even when the Fourier spectrum of such mapping is discrete, the spectrum of the flow can be singular continuous.

The listed examples of fractal Fourier spectra are purely deterministic. In physical observations, experiments and measurements, the stochastic component is present for obvious reasons: neither it is possible to ensure perfectly constant external conditions during the whole experiment, nor is the precision of the measurement tools infinite. Theoretical models also have limited accuracy, and contribution of non-accounted or neglected factors can be often viewed as some weak noise. Fractal sets which support singular continuous Fourier spectra, are fragile; it is natural to think that a weak disturbance should either make them discrete, collecting spectral measure into the countable atomic subset, or (which seems much more plausible) smooth out the singularities, turning them into the absolutely continuous ones. A natural question is: what (if anything) remains from the fractal patterns of underlying deterministic systems in the power spectra of noisy datasets ? Below we consider several of such situations. We show that the noise which enters the data only during the measurement, leaves intact large parts of the fractal structure of the spectral measure. Further, we investigate numerically how the mechanisms responsible for the singular continuous component of the Fourier spectrum are affected by the presence of additive noise. Although action of noise leads to the decay of correlations, on the intermediate stage the "noiseless" correlation patterns persist. Duration of this stage is related to the noise intensity by the power law.

The structure of the paper is as follows. In Sect. 2 we review the basic properties of fractal power spectra, describe the mechanisms of their onset and characterize the tools to be used in our studies. In Sect. 3 the contamination of fractal spectra by observational noise is discussed. In two following sections we examine numerically the action of additive noise on the fractal Fourier spectra of, respectively, geometric and dynamical origin. The paper ends with the brief discussion of the influence of randomness on spectral and correlation characteristics of self-similar symbolic sequences.

2 Fractal Fourier spectra in the absence of noise: definitions, examples and mechanisms

2.1 Basic notions

Let the sequence $\{x_j\}$, $j = 1, 2, 3, \ldots$ be a sufficiently long series of values of an observable x; this series can be obtained by iterating a mapping, by sampling equidistant points of the time-dependent solution of a differential equation, by experimental measurements separated by equal time intervals, etc. The finite-length Fourier sum is defined as

$$S(\omega, l) = \frac{1}{l} \langle | \sum_{k=m}^{m-1+l} x_k \mathrm{e}^{i2\pi k\omega} |^2 \rangle \tag{1}$$

where angular brackets denote averaging over the initial position m.

Let us increase the length of the sample l. If for almost all values of the frequency ω the spectral sums decay to zero, whereas for the remaining countable set of ω-values these sums grow proportionally to l and form in the coordinates ω, S the δ-peaks, the power spectrum is discrete (pure-point). If, on the contrary, for the fixed value ω_0 the sums $S(\omega_0, l)$ converge to the bounded non-zero value $S(\omega_0, \infty)$, and this value coincides with the limits of spectral sums for $\omega \to \omega_0\pm$, then the power spectrum is absolutely continuous at $\omega = \omega_0$.

A pure-point spectrum indicates to the regular (periodic or quasiperiodic) character of dynamics; absolutely continuous spectra are typical for chaotic and stochastic processes. The intermediate case between these two is the singular continuous power spectrum: for the zero-measure continuum of ω-values the finite spectral sums neither decay nor grow linearly with l; commonly they grow as l^α with $0 < \alpha(\omega) < 1$. Although the growth is unbounded, the singularities for these values of ω are weaker than δ-functions. Elsewhere the spectral sums decay, therefore in the case of "purely" singular continuous power spectrum the whole spectral measure sits on this disjoint fractal continuum.

Dynamics with fractal Fourier spectra has been detected in different deterministic dynamical systems. Naturally, introduction of noise broadens the singularities and turns the power spectrum into absolutely continuous. This process is a subject of our current research.

In the fragile situation in which the spectral measure is concentrated on the fractal support, numerical estimates in the frequency domain are not very secure. Computations in the time domain are more reliable; according to the Wiener-Khinchin theorem [10], there the counterpart of the power spectrum is the autocorrelation function. Below we will use this duality and in our numerical experiments employ mostly the normalized autocorrelation $C(\tau)$ which, for an observable x_j $(j = 1, 2, \ldots)$, is defined as

$$C(\tau) = \frac{\langle x_j x_{j+\tau}\rangle - \langle x_j\rangle^2}{\langle x_j^2\rangle - \langle x_j\rangle^2} \tag{2}$$

where averaging over the position j is performed.

For processes with discrete Fourier spectrum, the autocorrelation $C(\tau)$ displays repetitive peaks of unit or asymptotically unit height at arbitrarily large values of the argument. In case of purely absolutely continuous spectral measure, autocorrelation decays [10].

A further useful indicator is the integrated autocorrelation

$$C_{\mathrm{int}}(T) \equiv \frac{1}{T}\sum_{\tau=0}^{T} C^2(\tau) \tag{3}$$

Vanishing of $\lim_{T\to 0} C_{\mathrm{int}}(T)$ demonstrates the absence of discrete component in the power spectrum. For deterministic dynamical processes with singular continuous Fourier spectra, $C_{\text{int}}(T)$ decays, whereas the plot of $C(\tau)$ exhibits infinite series of non-decaying peaks of moderate (lower than unit) height.

Besides the qualitative criterion for the absence of discrete spectral component, the decay of integrated autocorrelation C_{int} is helpful for finding the quantitative characteristics of a multifractal spectrum: as shown in [11], asymptotically $C_{\text{int}}(T) \sim T^{-D_2}$ where D_2 is the correlation dimension of the spectral measure.

2.2 Thue-Morse symbolic sequence

The classical textbook example of a dynamical system with singular continuous spectrum is the Thue-Morse symbolic sequence [12, 13], defined on the alphabet of two symbols A and B. Of the many equivalent ways to obtain this sequence, we choose repeated concatenations. Let $\{\overline{w}\}$ denote the operation of inversion: replacement of each symbol in the binary word $\{w\}$ by the complementary one: A by B and vice versa. Take a word and write behind its last letter the inversion of this word. Such concatenation produces a word of the doubled length; by repeating this combination of inverting and abutting we obtain the word of quadruple length, etc. To arrive at the Thue-Morse sequence, the process starts with a single symbol and goes as follows:

$$A \Rightarrow AB \Rightarrow ABBA \Rightarrow ABBABAAB \ldots \tag{4}$$

On assigning numerical values (e.g. $A = 1$, $B = -1$) to symbols, the sequence becomes a data series which is neither periodic nor chaotic, and the support of its Fourier spectral measure is the singular continuous set [14]. As a prototype model combining self-similarity and weak disorder, the Thue-Morse sequence has found numerous applications in physics of one-dimensional patterns, both classical and quantum; a list of references can be found e.g. in the survey [15]. Most of the work is theoretical; in experiments the traces of spatial fractal spectra were detected in diffraction on specially prepared multilayer heterostructures [16, 17].

The Thue-Morse sequence is invariant under binary decimation (discarding every even symbol). Accordingly, the values of its autocorrelation function are interrelated by the recurrency

$$C(2t) = C(t), \quad C(2t+1) = -\frac{C(t) + C(t+1)}{2} \tag{5}$$

(with natural "initial condition" $C(0) = 1$); as can be seen in Fig.1(a), $C(t)$ is organized into a lattice which is nearly log-periodic in t, and its largest peaks form the geometric progression with the exponent 2. The relations (5) allow to estimate the decay rate of the integrated autocorrelation; in this way it has been shown that the correlation dimension of the fractal spectral measure equals $3 - \log(1 + \sqrt{17})/\log 2 = 0.64298\ldots$ [18].

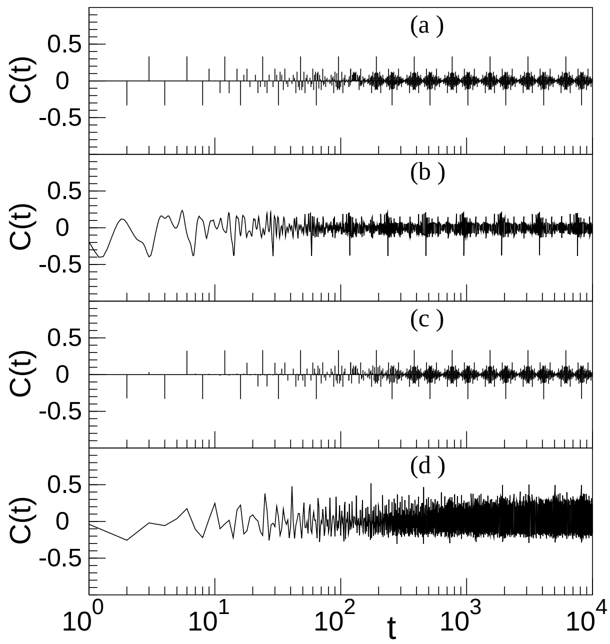

Figure 1: Autocorrelation for noiseless systems with fractal spectra:
(a) Thue-Morse symbolic sequence;
(b) Attractor of "homoclinic gluings": Eq.(6) at $a = 0$, $R = 15.823736676$, $D = 0.05263492319$ ($\nu = 2.0$);
(c) Mapping (6) at $\nu = 2, \mu = 1.401155189092$;
(d) Attractor of Eq.(6) with golden mean rotation number at $a = -0.56128733225$, $R = 14.148796862$, $D = 0.0543347619$ ($\nu = 1.50$).

Among the other examples of symbolic sequences with fractal Fourier spectra are generalizations of the Thue-Morse sequence obtained by combination of inversion with tripling ($w \to w\overline{w}\overline{w} \to \ldots$), quadrupling ($w \to w\overline{w}\overline{w}\overline{w} \to \ldots$) etc.

2.3 Two mechanisms behind fractal Fourier spectra in continuous dynamical systems

2.3.1 Model equations

A convenient example of a dissipative flow with singular continuous component in the power spectra is the set of 3 ordinary differential equations

$$\begin{aligned}\dot{x} &= \sigma(y-x)+\sigma Dy(z-R)\\ \dot{y} &= Rx-y-xz\\ \dot{z} &= xy-bz+ax\end{aligned} \qquad (6)$$

which models in the Lorenz approximation thermal convection caused by rapidly oscillating gravity field in a fluid layer [19]. The parameters σ, R and b have the same meaning as in the Lorenz equations, and we fix for σ and b the original values $\sigma = 10$ and $b = 8/3$ from the paper of Lorenz [20]. Additional (as compared to the Lorenz equations) terms in the first equation are proportional to the non-negative "vibrational parameter" D which characterizes the intensity of the gravity modulation; the purpose of the term ax in the 3rd equation is to violate the mirror symmetry of the system with respect to the transformation $(x, y) \Leftrightarrow (-x, -y)$.

Onset of chaos in Eq.(6) is related to homoclinic bifurcations: formation of structurally unstable homoclinic trajectories to the trivial equilibrium state. For $D < 1/R - 1/R^2$ the corresponding fixed point $x = y = z = 0$ is a saddle point with three real eigenvalues $\lambda_1 > 0 > \lambda_2 > \lambda_3$. The events which accompany the formation and breakup of a homoclinic orbit depend on the value of the saddle index ν: the ratio of eigenvalues $\nu \equiv -\lambda_2/\lambda_1$ [21].

At small values of D the inequality $\nu < 1$ holds, periodic orbits born from the destruction of the homoclinic trajectories are unstable, and the transition to chaos follows the scenarios of the unperturbed Lorenz model [22, 23].

We consider the complementary case: the parameter region $1/R-1/R^2-b(\sigma+1-b)/(\sigma R^2) < D < 1/R-1/R^2$ where the saddle index ν is larger than 1. This means that contraction in the vicinity of the saddle point prevails over the expansion, and the breakup of homoclinic trajectories creates stable periodic orbits. Evolution of these orbits from relatively simple to more and more complicated culminates in the birth of the strange attractor. As shown in [27], in the space of parameters D, R and a there is a continuum of qualitatively different routes to chaos, characterized by different scaling properties. We take just two of these routes, which exemplify the action of two different mechanisms in creating the fractal component of the spectrum.

2.3.2 Geometric mechanism

In the mirror-symmetric case $a = 0$ the increase of R is accompanied by the alternation of two kinds of bifurcations. One of these is the gluing bifurcation of stable periodic orbits: in the phase space two mirror-symmetric closed curves turn into two trajectories which are homoclinic to the same saddle-point; their subsequent breakup leaves a single stable closed curve of the doubled length. The other bifurcation is the symmetry-breaking of this new orbit which produces a new couple of mirror-symmetric stable periodic orbits. This process is infinitely repeated; its initial stages are sketched in Fig.2, and the projection of resulting self-similar attractor is shown in Fig. 3(a).

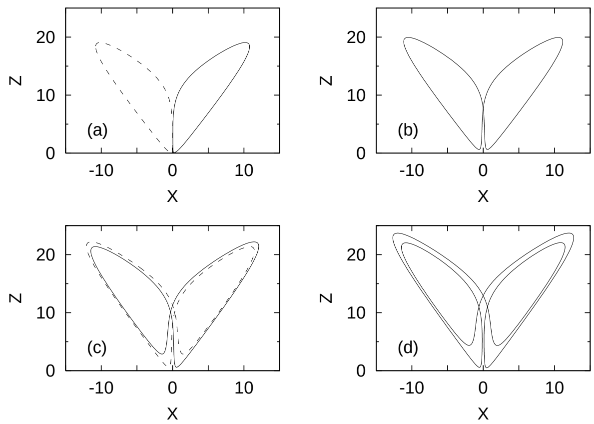

Figure 2: Bifurcation scenario of homoclinic gluings in Eq.(6) at $a = 0$:
(a) Two symmetric periodic orbits just before the 1st homoclinic bifurcation, $R = 12.5$, $D = 0.0630755$;
(b) Self-symmetric periodic orbit born from the 1st homoclinic bifurcation, $R = 13$, $D = 0.061275$;
(c) Two periodic orbits after the symmetry breaking, $R = 14.2$, $D = 0.0573078$;
(d) Self-symmetric periodic orbit born from the 2nd homoclinic bifurcation, $R = 15$, $D = 0.0549135$.

This scenario admits a simple symbolic description. Let the symbol A

denote a turn of the orbit in the subspace $x > 0$ and the symbol B, respectively, the turn in the subspace $x < 0$; then each orbit is encoded by a sequence of letters. To avoid ambiguity in the choice of initial point, for periodic orbits we start this sequence with the letter corresponding to the outermost turn. The symmetry transformation $x \to -x$, $y \to -y$ inverts the symbolic label of a trajectory. From this point of view, the gluing bifurcation concatenates two symbolic labels $\{w\}$ and $\{\overline{w}\}$ into the single label $\{w\overline{w}\}$, and the symmetry-breaking bifurcation does not change the labels of attracting orbits. The action of the whole scenario is thereby $A \Rightarrow AB \Rightarrow ABBA \Rightarrow ABBABAAB\ldots$ and the symbolic code of the attractor at the accumulation point is the Thue-Morse sequence. Therefore the autocorrelation function of the trajectory on this attractor, shown in Fig.1(b), has the same pattern as that of the Thue-Morse sequence: a log-periodic lattice with largest peaks separated by a factor 2.

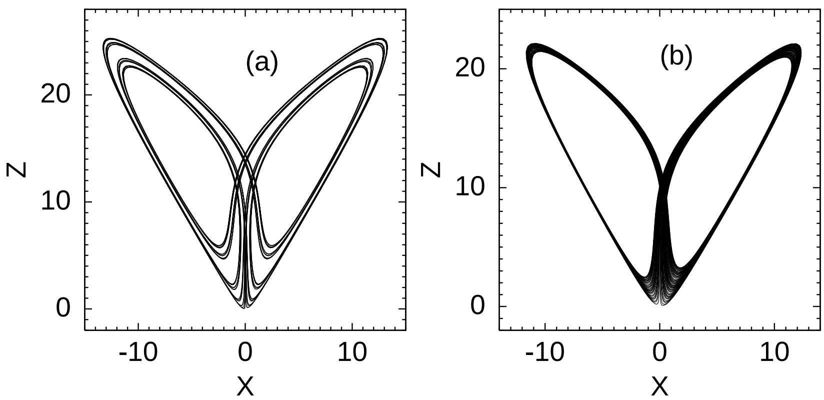

Figure 3: Attracting sets of Eq.(6):
(a) Attractor of the homoclinic gluing scenario, $a = 0$, $R = 15.823736676$, $D = 0.05263492319$;
(b) "Quasiperiodic" attractor with golden mean rotation number, $a = -0.56128733225$, $R = 14.148796862$, $D = 0.0543347619$.

Traditionally, a continuous flow close to homoclinicity is represented by the Poincaré mapping on the surface transversal to the stable manifold of the saddle point. Due to the strong contraction, this mapping can be reduced to the discontinuous 1-dimensional map which in the leading order has the structure

$$\xi_{i+1} = (|\xi_i|^\nu - \mu)\,\mathrm{sign}(\xi_i), \tag{7}$$

where ξ represents the coordinate along the local unstable manifold of the saddle, ν is the saddle index and μ is the active parameter. Families of maps of this kind were analyzed in [24, 19] where it was found that the bifurcation scenario had certain similarities to the period-doubling sequence of the logistic mapping, but also certain qualitative and quantitative distinctions. Renormalization treatment of the scenario shows that the universality class is uniquely defined by the value of the saddle index ν which completely predetermines the convergence rate of the bifurcation sequence and the geometrical scaling characteristics of the attractor. Denoting by A iterations with positive values of ξ and by B the negative ones, it is straightforward to see that the symbolic representation of the attracting set of (7) at the accumulation point of the bifurcation scenario is the Thue-Morse sequence. Not surprisingly, the autocorrelation function of this state, as plotted in Fig.1(c), bears very close resemblance to Fig.1(a).

In general, if the attracting set for a flow or a mapping admits a geometric partition whose symbolic description possesses fractal Fourier spectrum, the power spectrum of an orbit on this attractor should contain the singular continuous component. We interpret this as the geometric mechanism behind the onset of fractal spectra.

2.3.3 Dynamical mechanism

Setting $a \neq 0$ in Eq.(6) removes the mirror symmetry and enriches the dynamics. General descriptions of the variety of bifurcation sequences in families of flows close to the gluing bifurcation can be found in [25, 26, 27]; we concentrate on one particular scenario of transition to chaos. In a certain parameter domain the one-dimensional return mapping is equivalent to the circle map; this map has an inflection-like singularity of the order ν and is, in general, not one-to-one. It is convenient to introduce the rotation number ρ which has an apparent geometrical meaning: for closed trajectories ρ is a ratio of the number of turns in the positive half-space to the overall amount of turns, and for the non-closed ones ρ is a limit of this ratio for $t \to \infty$. The "subcritical domain" of the parameter space in which ρ is the same for almost all orbits, is separated by the "critical surface" from the supercritical one where the rotation number depends on initial conditions. Similarly to the parameter space of the usual circle map, the subcritical domain consists of the countable set of regions with rational values of ρ and the continuum of codimension-1 subsets with irrational values of the rotation number.

On the critical surface the return mapping becomes one-to-one, and the scenario of transition to chaos for irrational rotation numbers has much in common with the transition through quasiperiodicity [28]. Projection of the corresponding attracting orbit for the golden mean rotation number $\rho = (\sqrt{5}-1)/2$ is shown in Fig. 3. It can be seen that, unlike the Cantor-like attractor of the gluing scenario (cf. Fig.2), this orbit is dense on the transversal section. The one-dimensional return mapping induced by this orbit, is a homeomorphism of the circle with the golden mean rotation number, and the Fourier spectrum of this mapping is purely discrete. On the symbolic level, the encoding of the orbit is given by the Fibonacci symbolic sequence whose Fourier spectrum is discrete as well. However, as distinctly seen from the plot of the autocorrelation function of the orbit itself in Fig.1(d), the spectrum of the continuous-time process is not purely discrete: the peaks do not tend to 1, and there is an approximate periodicity on the logarithmic timescale. The distances between the highest peaks of $C(t)$ form a progression, with the exponent tending to $1/\rho$. We conclude that the power spectrum includes a singular continuous component.

The reason for the discrepancy between the spectral properties of the flow and of the Poincaré mapping induced by this flow, lies in the singular distribution of time intervals between consecutive returns of the orbit onto the Poincaré plane [7]. The saddle point at the origin belongs to the attractor, therefore a typical orbit in its motion over the attractor passes arbitrarily close to this equilibrium, and the return time exhibits a logarithmic divergence near the intersection of the Poincaré plane with the local stable manifold of the saddle point. The onset of the fractal spectral component is caused by slowing down of the motion near the saddle. This mechanism is specific for flows: obviously, it acts neither on mappings nor on symbolic sequences obtained from geometric partitions of the attractor, and it is natural to call it "dynamical mechanism". Every scenario of transition to chaos through homoclinic bifurcations ends up with the attractor on which typical orbits pass arbitrarily close to the saddle point infinitely many times (see e.g. [26, 27]); therefore the dynamical mechanism ensures presence of fractal component in the power spectra of flows at the accumulation points of all such scenarios. Naturally, this holds also for the scenario of homoclinic gluings in Eq.(6) discussed in Sec.2.3.2 above; however, in the cases in which both mechanisms is present, the geometric mechanism is the strongest of the two, and its contribution dominates the spectra of observables built with the help of variables participating in the symmetry transformation.

3 Contamination by instrumental noise

In this short section, we treat the situation in which the noise does not affect the nature of the process and interferes only at the observation stage by means of an inaccurate measurement device. Let observable be a superposition of the original signal x_i and δ-correlated noise ζ. In case of additive measurement noise, autocorrelation function for the variable $y_i = x_i + \zeta_i$ is

$$C_y(\tau) = \frac{C_x(\tau)}{1 + \langle\zeta_i^2\rangle / \langle x_i^2\rangle} \tag{8}$$

where $C_x(\tau)$ is the autocorrelation for the variable x_i.

For the noisy "amplitude modulation" $y_i = x_i(1 + \zeta_i)$, we get

$$C_y(\tau) = \frac{C_x(\tau)}{1 + \langle\zeta_i^2\rangle} \tag{9}$$

In both cases the autocorrelation function of the noisy observable is obtained from the autocorrelation of the original signal by uniform (τ-independent) contraction. The contraction factor depends on the distribution of noise and is non-zero for the noise with bounded mean square amplitude.

Accordingly, the integrated autocorrelation $C_{\rm int}(\tau)$ of the observable y_i differs from $C_{\rm int}(\tau)$ of x_i by the constant factor, and has the same decay rate. Hence, the correlation dimension D_2 of the spectral measure of y_i coincides with D_2 of the spectral measure of x_i. Furthermore, all generalized dimensions D_q with integer $q \geq 2$ for the spectral measure are prescribed by the growth rate of products of values of the autocorrelation function [29]; hence, if the power spectrum of x_i is multifractal, this multifractality in the domain $q \geq 2$ is quantitatively reproduced by the power spectrum of the observed variable y_i. On the other hand, the signal y_i includes the noisy component ζ; since the power spectrum of the latter is absolutely continuous, $D_q = 1$ for $q \leq 1$.

Now consider the instrumental noise on the symbolic level: in the course of observation some of the symbols can be identified wrongly. Let $X = x_1x_2x_3...$ and $Y = y_1, y_2, y_3 \ldots$ be binary symbolic strings:

$$y_i = \begin{cases} x_i & \text{with probability } \ 1-p \\ \overline{x_i} & \text{with probability } \ p \end{cases} \tag{10}$$

where $\overline{A}$, as above, denotes a symbol complementary to A. Then: $C_y(\tau) = (1-2p)^2\, C_x(\tau)$. For $p \neq \frac{1}{2}$ the pattern of $C_x(\tau)$ is uniformly vertically compressed. Accordingly, if the spectral measure of original symbolic sequence

X is fractal, its qualitative and quantitative structure for $q \geq 2$ is recovered in the measured symbolic signal Y. An example: if each individual symbol in the Thue-Morse sequence is "flipped" with probability $p \neq \frac{1}{2}$, the correlation dimension of the Fourier spectral measure of the resulting symbolic sequence remains equal to the "noiseless" value $D_2 = 3 - \log(1+\sqrt{17})/\log 2$.

4 Interaction between additive noise and geometric mechanism

4.1 Changes in the pattern of autocorrelation

Now let us allow the noise to interfere into dynamics. This inevitably leads to the onset of absolutely continuous spectral background and ultimate decay of autocorrelation. However, as we will see, in the pattern of autocorrelations it is possible to recover certain "remnants" which permit to conclude that the power spectrum of purely deterministic process is singular continuous. This effect is especially well pronounced in the situations when the fractal spectral component owes to the geometric mechanism. To elucidate this, consider the noisy version of the Eq.(6)

$$\begin{aligned} \dot{x} &= \sigma(y-x) + \sigma D y(z-R) + E\zeta(t) \\ \dot{y} &= Rx - y - xz \\ \dot{z} &= xy - bz \end{aligned} \tag{11}$$

with the values of the parameters σ, D, R, b corresponding to the accumulation of homoclinic gluings. Here, E is the amplitude of the noisy term, and $\zeta(t)$ is a random variable; for computational reasons it is convenient to take the variable uniformly distributed on the interval $(-1, 1)$.

Recall that in the absence of noise the universal properties of the bifurcation scenario are entirely determined by the saddle index $\nu = |\lambda_2|/\lambda_1$: the ratio of two eigenvalues of the linearization of the flow near the trivial equilibrium $x = y = z = 0$; to enable the sequence of homoclinic gluings, the inequality $\nu > 1$ should hold. To single out the action of the geometric mechanism, we consider observables built from the variable x. Reduction of the deterministic flow to one-dimensional mapping on the Poincaré plane yields the discontinuous recursion relation (7). At the accumulation point of the bifurcation sequence, the Fourier spectrum of this map is singular continuous due to the geometric mechanism. The noisy counterpart of Eq.(7) is

$$\xi_{i+1} = (|\xi_i|^\nu - \mu + E\zeta_i\,)\,\mathrm{sign}(\xi_i), \qquad (12)$$

ζ_i being a random function of the discrete argument.

In the deterministic case the attracting sets of Eq.(11) and Eq.(12) are self-similar and possess scaling properties. Introduction of noise "washes out" the fine structure of the attractors, and the approximate self-similarity can be recovered only beyond a certain level of resolution. The very same process takes place when additive noise acts on dynamical systems at the onset of chaos through period-doublings. It is convenient to characterize the system by means of its noise sensitivity β which has a transparent meaning: in order to be able to resolve each next level of the fine structure of the attracting set (that is, to see twice as many "bands" in the attractor of the flow, or twice as many "clusters" in the attractor of the map), the noise level should be reduced by a factor β. The value of $\beta = 6.61\ldots$ for the period-doubling scenario was found by direct computations and with the help of the renormalization formalism [30, 31].

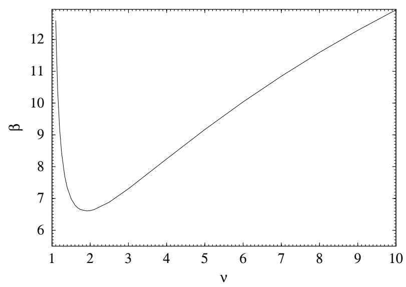

Figure 4: Sensitivity to noise as function of the saddle index ν.

Since both the period-doubling scenario and the onset of chaos through the gluings can be described within the framework of the same renormalization operator (see e.g. [19, 24, 26, 27]), under the given value of ν the sensitivity to noise for the discontinuous mapping (12) is characterized by the same value of β as for continuous unimodal mapping $\xi_{i+1} = |\xi_i|^\nu - \mu + E\zeta_i$. Whereas in the discontinuous case all values of ν are equally relevant, for non-degenerate continuous mappings only the quadratic extrema (ν=2) are important. The numerically found dependence $\beta(\nu)$ is shown in Fig.4; to our knowledge this is the first computation for $\nu \neq 2$. It turns out that the systems with $\nu \approx 2$ are the least sensitive ones: the minimum is reached at $\nu \approx 1.91$.

The action of noise on the pattern of autocorrelation function of the mapping (12) is illustrated in Fig.5; the value $\nu = 2$ chosen for this set of computations, corresponds to the sensitivity $\beta = 6.61904\ldots$ in the curve of Fig. 4. The plot in Fig.5(a) presents numerically evaluated autocorrelation for the noise with the amplitude $E_0 = 10^{-11}$, and the lower panels (b), (c), (d), (e) and (f) correspond to the intensities of noise βE_0, $\beta^2 E_0$, $\beta^3 E_0$, $\beta^4 E_0$ and $\beta^5 E_0$, respectively.

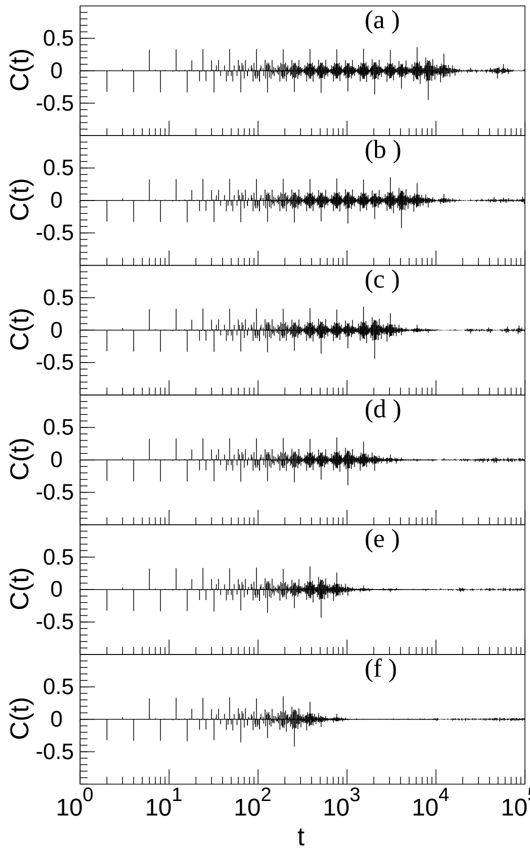

Figure 5: Autocorrelation for the mapping (12) with ν=2:
(a) $E = E_0 = 10^{-11}$; (b) $E = \beta E_0 = 6.61904 \times 10^{-11}$;
(c) $E = \beta^2 E_0 = 4.38117 \times 10^{-10}$; (d) $E = \beta^3 E_0 = 2.89991 \times 10^{-9}$;
(e) $E = \beta^4 E_0 = 1.91946 \times 10^{-8}$; (f) $E = \beta^5 E_0 = 1.27050 \times 10^{-7}$.

The plots demonstrate that the original log-periodic pattern of autocorrelation persists almost intact until a certain threshold value of time $t_{\rm n}$; beyond t_n autocorrelation rapidly decays. In subplots (a)-(f) each increase of the noise intensity by the factor β is accompanied by the shift of the right boundary of the correlation pattern "one big peak to the left": in other words, $t_{\rm n}$ is decreased by factor 2. Accordingly, the length of time interval during which the autocorrelations largely behave in the same way as in the absence of noise, is related to the noise intensity by means of the power law:

$$t_{\rm n} \approx C E^{-\kappa}, \quad \kappa \equiv \frac{\log \beta(\nu)}{\log 2} \tag{13}$$

This is also corroborated by computations for other values of ν.

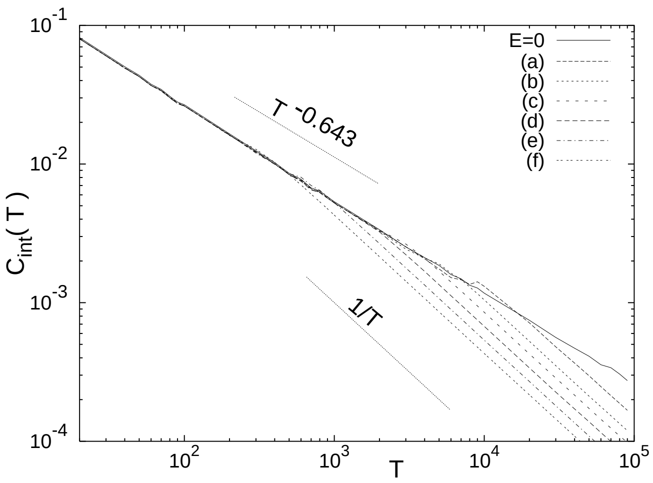

Figure 6: Integrated autocorrelation for the mapping (12) with ν=2. Solid line: absence of noise; (a)-(f): noise intensities as in Fig.5.

The abrupt breakdown of the intermediate "noiseless" asymptotics and the onset of dependency corresponding to the absolutely continuous spectrum is visible also in the decay of the integrated autocorrelation. Until $T \approx t_{\rm n}$, the law $C_{\rm int}(T) \sim T^{-D_2}$ holds; here D_2 is the correlation dimension of the power spectrum in the absence of noise which for the mapping (12) within numerical accuracy coincides with the value $0.642\ldots$ of the Thue-Morse sequence. For $T > t_{\rm n}$ the decay law switches abruptly to $C_{\rm int}(T) \sim T^{-1}$, disclosing the absence of fractal structure at the "microscopic" level of the spectrum. This crossover behavior is demonstrated in Fig.6 which shows in the logarithmic coordinates the plots of $C_{\rm int}(T)$ for different noise intensities. The curves detach from the noiseless asymptote; for the geometric progression of noise intensities with the factor β, they tend to the equidistant grid of straight lines separated by the distance $2^{-1/2}(1-D_2)\log 2$.

The very similar behavior is found in case of continuous-time dynamics. Results obtained by numerical integration of Eq.(11) under different values of the noise amplitude E are presented in Fig.7: each multiplication of E by the factor β results in the disappearance of the rightmost large peak and an island around it. Again we observe the persistence of the pattern of the

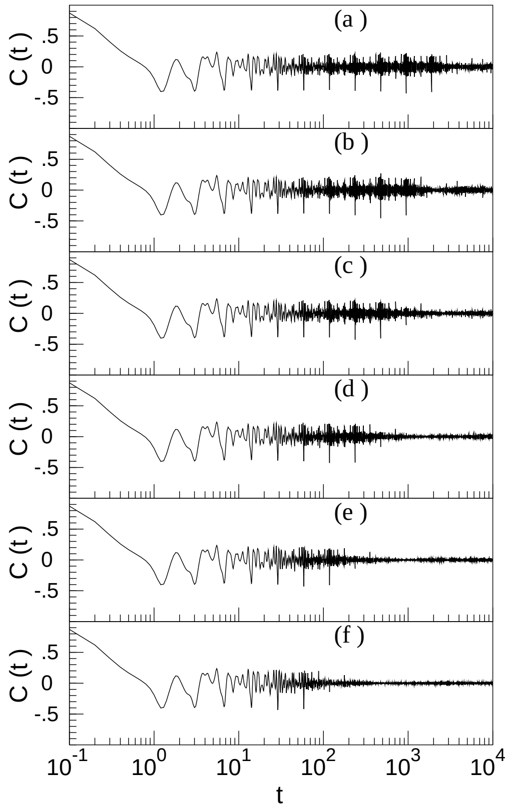

Figure 7: Autocorrelation for the equations (11) with ν=2:
(a) $E=E_0=10^{-8}$; (b) $E=\beta E_0=6.61904\times 10^{-8}$;
(c) $E=\beta^2 E_0=4.38117\times 10^{-7}$; (d) $E=\beta^3 E_0=2.89991\times 10^{-6}$;
(e) $E=\beta^4 E_0=1.91946\times 10^{-5}$; (f) $E=\beta^5 E_0=1.27050\times 10^{-4}$.

autocorrelation function within a certain interval of time, whose duration is interrelated with the noise intensity by means of the power law (13). The decay of integrated autocorrelation, shown in Fig.8, also demonstrates the familiar picture of crossover from the noiseless asymptotics with a fractional power to the decay law T^{-1}; curves corresponding to different amplitudes of noise tend to a regular grid of parallel lines.

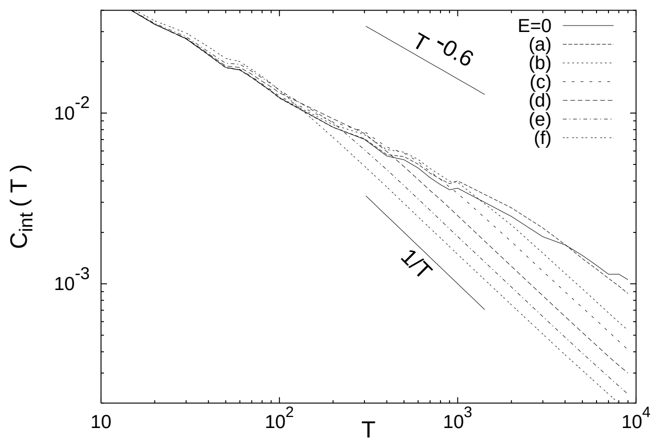

Figure 8: Integrated autocorrelation for the flow (11). Parameter values as in Fig.3(a). Solid line: absence of noise; (a)-(f): noise intensities as in Fig.7.

Under the same value of ν the same values of β characterize the washing out of the correlation pattern for the discrete mapping (12) and continuous flow (11). This confirms the quantitative universality of the phenomenon and allows us to expect that the same scaling of the length $t_{\rm n}$ of "singular continuous" autocorrelation pattern can be measured in sufficiently accurate real physical experiments by introducing the controlled amount of noise.

It should be noted that, strictly speaking, the value of sensitivity depends on the particular kind of noise [32, 33]. The procedure employed for the calculations in Fig. 4 assumes that the noise is Gaussian. However, from the above numerical results on the scaling of autocorrelation functions it appears that the values of sensitivity with respect to uniformly distributed random variables are close to the corresponding values for Gaussian noise.

4.2 Changes in the shape of spectral curves

Estimates of autocorrelation serve as indirect evidence on the structure of the Fourier spectrum. Directly, the implications of noise in the frequency domain can be visualized with the help of the finite-length Fourier sums (1). In Fig. 9(a,b) these sums are estimated in the whole relevant interval $0 \leq \omega \leq 1/2$ for the noiseless mapping (7) and the mapping (12) with rather weak noise ($E = 10^{-11}$) respectively. Results are obtained by averaging over 2^9 sums evaluated for orbit segments of the length 2^{15} .

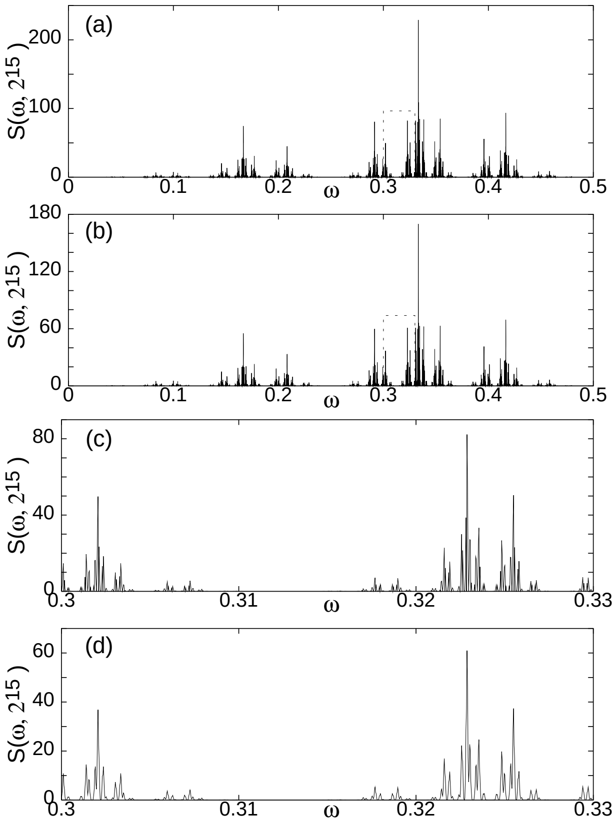

Figure 9: Spectral sums for the mapping (12) with ν=2. (a) $E = 0$; (b) $E = 10^{-11}$; (c) magnification of rectangle with dashed border from (a); (d) magnification of rectangle with dashed border from (b).

On this scale both sets seem fractal, and the only visible difference is the somewhat lower magnitude of the peaks in (b), compared to their counterparts in (a). However, the blowup for a smaller interval of values of ω in subplots (c,d) reveals the striking difference: the peaks in the spectral sum of the noiseless map retain their δ-like shape, whereas the sum in (d) displays continuous background around the finite-width peaks.

Difference between the structure of spectral sums in the absence and in the presence of noise is especially well seen in the logarithmic coordinates by comparison of sums for different sample length l (Fig.10 and Fig.11).

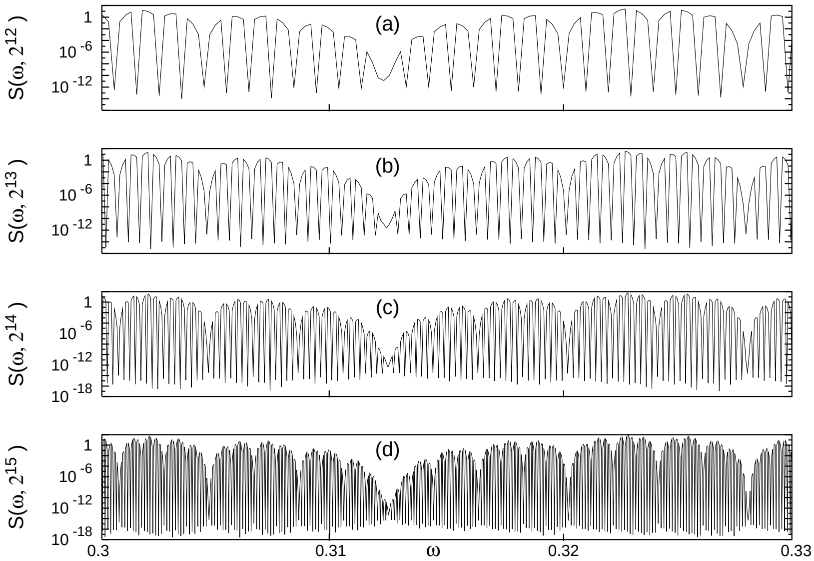

Figure 10: Spectral sums for the noiseless map (7) with different sample length l: (a) $l = 2^{12}$; (b) $l = 2^{13}$; (c) $l = 2^{14}$; (d) $l = 2^{15}$.

Increase of l provides better resolving of the spectral measure. In particular, we observe that the new and new narrow deep "holes" with bottom values near the limit of numerical resolution appear on the spectral background. Let us start with the noiseless mapping. As seen from Fig.10(a-d), in the absence of noise each doubling of l is accompanied by the doubling of the number of these "holes": when l is doubled, a new hole appears in the middle of each interval between two adjacent old ones. This can be traced back to the spectral measure of the Thue-Morse sequence: in that case the finite-length Fourier sums are given by the product [34]

$$S(\omega, 2^n) = \prod_{k=1}^{n} (1 - \cos 2^{k+1}\pi\omega) \tag{14}$$

By virtue of this expression, $S(\omega, 2^{n+1})$ has twice as many zeroes as $S(\omega, 2^n)$, and the additional zeroes of the former are located exactly in the middle of intervals between the adjacent zeroes of the latter. As a result, there is no convergence: in the limit $n \to \infty$ the spectral curve tends to zero almost everywhere, besides the zero-measure dense set of singularities.

Now let us introduce the weak noise. For n small enough, the initial transformations of finite-length spectral sums $S(\omega, 2^n)$ do not bring qualitative changes: the curves in Fig.11(a,b) almost do not differ from their respective counterparts in Fig.10(a,b). However, starting from $n = 14$ the similarity to the noiseless case breaks down: the number of holes does not grow, and the pattern starts to acquire its final shape (Fig.11(c,d)). This is a beginning of the process of convergence to a limiting spectral curve $S(\omega, \infty)$ which, albeit markedly non-smooth, is absolutely continuous.

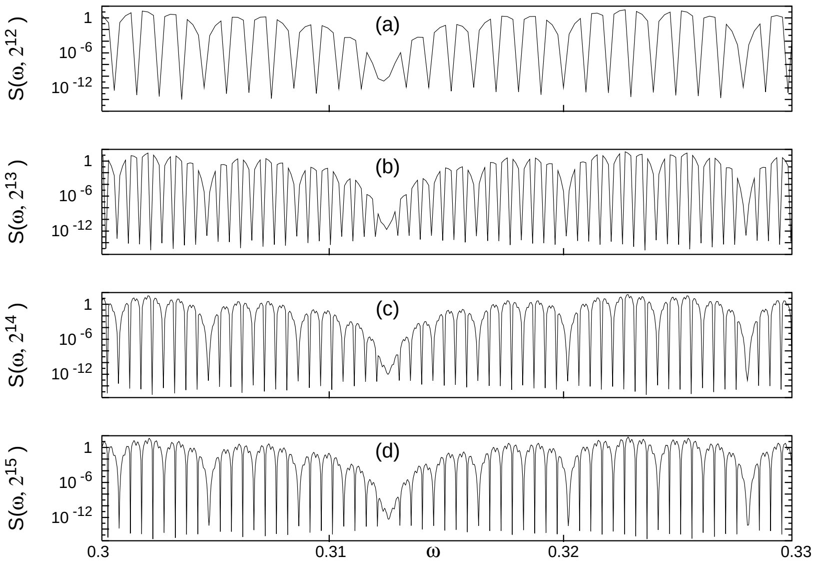

Figure 11: Spectral sums for the mapping (12) with $E = 10^{-11}$ and different sample length l: (a) $l = 2^{12}$; (b) $l = 2^{13}$; (c) $l = 2^{14}$; (d) $l = 2^{15}$.

The higher is the amplitude of the noisy term, the earlier starts the decline of spectral curves from the infinite process of division of intervals depicted in Fig.10. This process is characterized by scaling properties as well: each increase of the noise intensity by the factor β halves the maximal length l_m at which the last new holes appear on the spectral bottom. For $E = 10^{-11}$, as seen from Fig.11, $l_m = 2^{13}$; for $E = 6.619 \times 10^{-11}$ the threshold length is $l_m = 2^{12}$, for $E = \beta^2 \times 10^{-11}$ the last holes appear at $l_m = 2^{11}$ and so on.

5 Noise versus dynamical mechanism: slow exponential decay of correlations

To check the influence of noise on the singular continuous spectral component created by the action of the dynamical mechanism, we consider the equations (11) at the parameter values which, in the absence of noise, correspond to the attractor with golden mean rotation number presented in Fig.3(b).

On the whole, the autocorrelation function appears to be more robust, and one needs much higher amplitudes of noise (compared to the fractal spectra of geometric origin) in order to enforce the decay of correlations at relatively low time values. Typical patterns are presented in Fig.12.

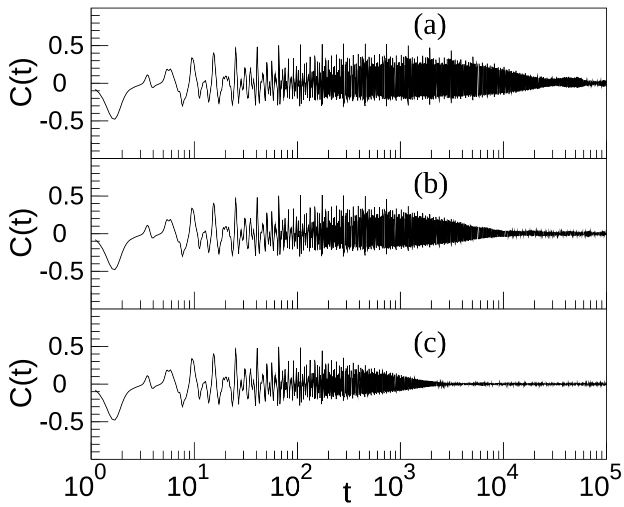

Figure 12: Autocorrelation for the noisy equations (11) with "quasiperiodic" attractor at ν=1.5:
(a) $E = 10^{-4}$; (b) $E = 10^{-3}$; (c) $E = 10^{-2}$.

In many respects, the picture seems familiar and reminds the influence of noise on the autocorrelation in the case of geometric mechanism: within a certain time interval $t_{\rm n}$ the log-periodic pattern of the noiseless case is preserved, and the length of this interval is related to the noise amplitude by means of the power law. An important difference, however, is the behavior outside the boundary of this interval. Whereas in case of the geometric mechanism the autocorrelation beyond $t_{\rm n}$ rapidly collapsed, in the subplots of Fig.12 we see a very slow gradual decay of autocorrelation between $t_{\rm n}$ and $\sim 10t_{\rm n}$. Fig.13 shows the evolution of the "envelope" of the autocorrelation function: the curve drawn through the local maxima of $|C(t)|$. According to these plots, the decay of the autocorrelation function is, on the average, exponential.

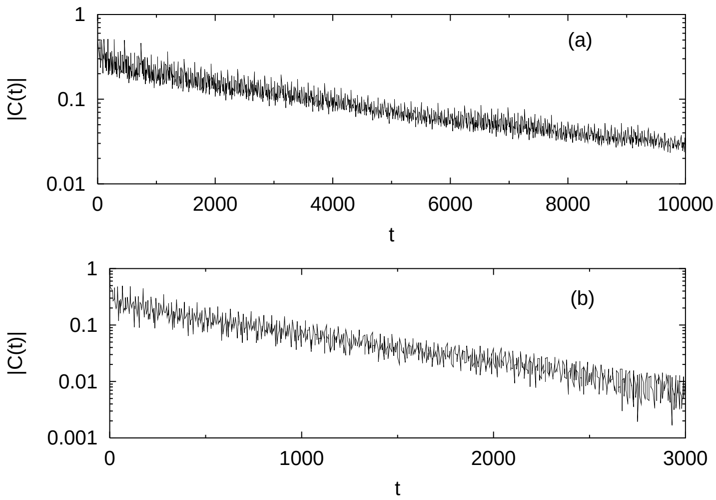

Figure 13: Decay of the envelope of $|C(t)|$: (a) $E = 10^{-3}$; (b) $E = 10^{-2}$.

Numerical estimation of finite-length spectral sums shows that restructurings in the frequency domain, caused by the action of noise, qualitatively resemble the changes which have been described for the geometric mechanism (Sect.4.2). In the absence of noise the growth of the sample length l leads to infinite "roughening" and fragmentation of spectral curves $S(\omega, l)$. When the noise is present, the initial stages of the increase of l are accompanied with same fragmentation and "roughening" of curves; however, this process ends after finitely many steps, and the further increase of l does not modify the spectral curves significantly.

6 Discussion

The above results demonstrate that in the situations in which noise becomes a non-negligible dynamical factor, singular continuous power spectra turn into absolutely continuous ones. At the same time, the pattern of the autocorrelation function retains large segments of the structures which are typical for the dynamics with fractal Fourier spectra. Presence of such segments in the estimates of autocorrelation (and, further, scaling of their lengths with respect to the noise intensity) provide reliable indication to the presence of singular continuous component in the power spectra of non-disturbed systems.

For fractal spectra caused by geometrical mechanism, yet another kind of noise can be relevant: this is the random influence "on the symbolic level" which distorts the self-similar pattern of the underlying symbolic dynamics. There are different formal ways to introduce such influence; we mention here just two possibilities, using the Thue-Morse symbolic sequence as a convenient example. This sequence, as it has been defined in Sect.2.2, is obtained by alternating inversions and concatenations. Randomness can enter this process in the following way: at each step the word $\{w\}$ is concatenated either with itself (producing the word $\{ww\}$ or with its inversion (producing the word $\{w\overline{w}\}$). On assigning the probabilities p to the first event and $1-p$ to the second event respectively, we see that setting $p=0$ creates the Thue-Morse sequence whereas $p=1$ results in the trivial repetition of symbols. For $p \neq 0, 1$ the process is random. After each event the length of the sequence is doubled, and the finite-length Fourier sums evolve according to

$$S(\omega, 2^{n+1}) = S(\omega, 2^n) \times \left\{ \begin{array}{ll} (1+\cos 2^{n+1}\pi\omega) & \text{with probability} \quad p \\ (1-\cos 2^{n+1}\pi\omega) & \text{with probability } 1-p \end{array} \right. \tag{15}$$

Incorporating this expression into the multifractal formalism developed in [29], the estimation of the correlation dimension D_2 of the spectral measure is reduced to the the computation of the random matrix product. Let M be the 2×2 matrix $\begin{pmatrix} 3/2 & \pm 1 \\ 1/2 & \pm 1 \end{pmatrix}$ where the right column is chosen to be positive with probability p and negative with probability $1-p$, and let $\lambda(n)$ be the largest of two eigenvalues of the product of n randomly picked matrices M. Then

$$D_2 = 1 - \frac{1}{2} \lim_{n\to\infty} \frac{\log \lambda(n)}{n} \tag{16}$$

The function $D_2(p)$ is presented in Fig.14; it monotonically decreases from $D_2(0) = 0.6429\ldots$ to $D_2(1) = 0$.

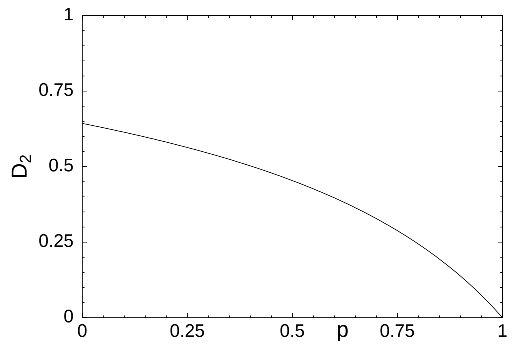

Figure 14: Correlation dimension of spectral measure for a random combination of concatenations and binary inversions.

It should be kept in mind that Eq.(16) predicts the average value for the infinite ensemble of infinitely long symbolic strings produced by random concatenations; since the corresponding dynamical system is not ergodic, the estimate of D_2 in an individual long symbolic sequence should not necessarily tend to this average value.

One of the alternative ways to obtain the Thue-Morse sequence is based on repetitive substitutions (inflations): every symbol A of the code is simultaneously replaced by the combination AB, and every symbol B, respectively, by BA. Randomness can be introduced into this scheme e.g. by means of "mutations" when for some symbols the substitutions decline from the prescribed general rule; the choice among the different substitution patterns can be characterized through probabilities. The case when these probabilities are independent of the position in the symbolic string, was treated in [35]; it has been shown that mutations lead to the power-law decay of autocorrelation, and that the multifractal component of the spectral measure persists if the probability of mutations is low enough. Power law decay of correlations ("long-range correlations") are ubiquitous in physics of critical phenomena [36] as well as in diverse data of biological [37, 38, 39, 40, 41], geophysical [42, 43] etc. origin; it would be challenging to find out whether in some of these cases the origin of such correlations is related to weak random violations of the intrinsic symbolic dynamics with fractal power spectra.

Acknowledgements

I am grateful to Arkady Pikovsky, Jürgen Kurths and Antonio Politi for fruitful discussions.

References

[1] J. P. Gollub, H. L. Swinney, Onset of turbulence in a rotating fluid, Phys. Rev. Lett., **35**, 927–930 (1975).

[2] J. P. Gollub, S. V. Benson, Many routes to turbulent convection, J. Fluid Mech., **100**, 449–470 (1980).

[3] M. Reed, B. Simon, *Methods of modern mathematical physics*, Academic Press, NY, 1972.

[4] R. del Rio, S. Zhitomirskaya, N. Makarov, B. Simon, Singular continuous spectrum is generic, Bull. Amer. Math. Soc. **31**, 208–212 (1994).

[5] A. S. Pikovsky, U. Feudel, Correlations and spectra of strange non-chaotic attractors, J. Phys. A **15**, 5209–5219 (1994).

[6] A. S. Pikovsky, U. Feudel, A. Politi, Renormalization of correlations and spectra of a strange nonchaotic attractor, J. Phys. A: Math.,Gen. **29**, 5297–5311 (1996).

[7] A. S. Pikovsky, M. A. Zaks, U. Feudel, J. Kurths, Singular continuous spectra in dissipative dynamical systems, Phys. Rev. E **52**, 285–296 (1995).

[8] M. A. Zaks, A. S. Pikovsky, J. Kurths, Steady viscous flow with fractal power spectrum, Phys. Rev. Lett. **77**, 4338–4341 (1996).

[9] M. A. Zaks, Fractal Fourier spectra of Cherry flows, Physica D **149** (2001), 237–247 (2001).

[10] I. P. Cornfeld, S. V. Fomin, Ya. G. Sinai, *Ergodic Theory* (Springer, New York, 1982).

[11] R. Ketzmerick, G. Petschel, T. Geisel, Slow decay of temporal correlations in quantum systems with Cantor spectra, Phys. Rev. Lett. **69**, 695–698 (1992).

[12] A. Thue, Über unendliche Zeichenreihen, Norske vid. Selsk. Skr. I. Mat. Nat. Kl. Christiania **7**, 1–22 (1906).

[13] M. Morse, Recurrent geodesics on a surface of negative curvature, Trans. A. M. S. **22**, 84–100 (1921).

[14] K. Mahler, On the translation properties of a simple class of arithmetical functions, J. Math. and Phys. **6**, 158–163 (1926).

[15] A. Bovier, J.-M. Ghez, Remarks on the spectral properties of tight-binding and Kronig-Penney models with substitution sequences, *J. Phys. A: Math., Gen.* **28**: 2313-2324 (1995).

[16] F. Axel and H. Terauchi, High-resolution X-ray-diffraction spectra of Thue-Morse GaAs-AlAs heterostructures: towards a novel description of disorder, *Phys. Rev. Lett.* **66**: 2223-2226 (1991).

[17] J. Peyrière, E. Cockayne, F. Axel, Spectra of finite-size Thue-Morse GaAs-AlAs multilayer heterostructures, *J. de Phys. I* **5**: 111-128 (1995).

[18] M. A. Zaks, A. S. Pikovsky, J. Kurths, On the correlation dimension of the spectral measure for the Thue-Morse sequence, J. Stat. Phys. **88**, 1387–1392 (1997).

[19] D. V. Lyubimov, M. A. Zaks, Two mechanisms of the transition to chaos in finite-dimensional models of convection, Physica D **9**, 52–64 (1983).

[20] E. N. Lorenz, Deterministic nonperiodic flow, J. Atmos. Sci. **20**, 130–141 (1963).

[21] P. Glendinning, *Stability, instability and chaos: an introduction to the theory of nonlinear differential equations* (Cambridge Univ. Press, Cambridge, 1994),

[22] V. S. Afraimovich, V. V. Bykov, L. P. Shilnikov, On the appearance and the structure of the Lorenz attractor, Sov. Phys. Doklady **22**, 253–255 (1977).

[23] C. Sparrow, *The Lorenz Equations: Bifurcations, Chaos, and Strange Attractors* (Springer, Berlin, 1982).

[24] A. Arneodo, P. Coullet, C. Tresser, A possible new mechanism for the onset of turbulence, Phys. Lett. A **81**, 197–201 (1981).

[25] J.-M. Gambaudo, I. Procaccia, S. Thomae, C. Tresser, New universal scenarios for the onset of chaos in Lorenz-type flows, Phys. Rev. Lett **57**, 925–928 (1986).

[26] I. Procaccia, S. Thomae, C. Tresser, First return maps as a unified renormalization scheme for dynamical systems, Phys. Rev. A **35**, 1884–2001 (1987).

[27] D. V. Lyubimov, A. S. Pikovsky, M. A. Zaks, Universal scenarios of transition to chaos via homoclinic bifurcations, Mathematical Physics Review, vol.**8**, edited by S. P. Novikov (Gordon and Breach, Chur, 1989), 221–292.

[28] M. A. Zaks, Scaling properties and renormalization invariants for the "homoclinic quasi-periodicity", Physica D **62**, 300–316 (1993).

[29] M. A. Zaks, A. S. Pikovsky, J. Kurths, On the generalized dimensions for the Fourier spectrum of the Thue-Morse sequence, J. Phys. A: Math.Gen. **32**, 1523–1530 (1999).

[30] J. Crutchfield, M. Nauenberg, J. Rudnick, Scaling for external noise at the onset of chaos, Phys. Rev. Lett. **46**, 933–935 (1981).

[31] B. Shraiman, C. E. Wayne, P. C. Martin, Scaling theory for noisy period-doubling transitions to chaos, Phys. Rev. Lett. **46**, 935–939 (1981).

[32] A. Hamm and R. Graham, Quasipotentials for simple noisy maps with complicated dynamics, J. Stat. Phys. **66**, 689–725 (1992).

[33] A. Hamm and R. Graham, Scaling for small random perturbations of golden critical circle maps, Phys. Rev. A **46**, 6323–6333 (1992).

[34] C. Godrèche, J. M. Luck, Multifractal analysis in reciprocal space and the nature of the Fourier transform of self-similar structures, J. Phys. A: Math., Gen. **23**, 3769–3797 (1990).

[35] M. A. Zaks, Multifractal Fourier spectra and power-law decay of correlations in random substitution sequences, *accepted by* Phys. Rev. E (2001).

[36] H. E. Stanley, S. V. Buldyrev, A. L. Goldberger, S. Havlin, C.-K. Peng, M. Simons, Long-range power-law correlations in condensed matter physics and biophysics, Physica A **200**, 4–24 (1993).

[37] C.-K. Peng, S. V. Buldyrev, A. L. Goldberger, S. Havlin, F. Sciortino, M. Simons, H. E. Stanley, Long-range correlations in nucleotide sequences, Nature **356**, 168–170 (1992).

[38] W. Li, K. Kaneko, Long-range correlation and partial $1/f^\alpha$ spectrum in a noncoding DNA sequence, Europhys. Lett. **17**, 655–660 (1992).

[39] B. Audit, C. Thermes, C. Vaillant, Y. d'Auberon-Carafa, J. F. Muzzy, A. Arneodo, Long-range correlations in genomic DNA: a signature of the nucleosomal structure, Phys. Rev. Lett. **86**, 2471–2474 (2001).

[40] J. M. Hausdorff, C.-K. Peng, Z. Ladin, J. Wei, A. Goldberger, Is walking a random walk ? Evidence for long-range correlations in stride interval of human gait, J. Appl. Physiol. **78**, 349–358 (1995).

[41] M. Duarte, V. Zatsiorsky, Long-range correlations in human standing, Phys. Lett. A **283**, 124–128 (2001).

[42] E. Koscielny-Bunde, A. Bunde, S. Havlin, H. E. Roman, Y. Goldreich, H.-J. Schellnhuber, Indication of a universal persistence law governing atmospheric variability, Phys. Rev. Lett. **81**, 729–731 (1998).

[43] R. B. Govindan, D. Vjushin, S. Brenner, A. Bunde, S. Havlin, H.-J. Schellnhuber, Long-range correlations and trends in global climate models: comparison with real data, Physica A **294**, 239–248 (2001).